Green Chemistry

PAPER

View Article Online
View Journal

Cite this: DOI: 10.1039/d5gc06094j

O-Demethylation of biobased anisole-like derivatives induced by acoustic energy: role of the cavitation bubble–water interface

Kafui Y. E. Late,[a] Damien Denis,[a] Prince N. Amaniampong,[a] Tony Chave,[b] Jorge A. Delgado[c] and François Jérôme *[a]

Received 14th November 2025,
Accepted 26th January 2026

DOI: 10.1039/d5gc06094j

rsc.li/greenchem

Using the *O*-demethylation of syringol as a model reaction, we investigated and clarified the reaction mechanism occurring at the cavitation bubble–water interface. By combining kinetic data, experimental tests, and product analysis, we demonstrated that water at this interface reaches a supercritical state, with a roughly estimated temperature of around 400° ± 35 °C. Under these conditions, syringol mainly undergoes thermal cracking, predominantly forming 3-methoxycatechol. By controlling the solution temperature and the nature of the gaseous atmosphere, we were able to modulate the energy released at the bubble collapse time, thereby minimizing over-cracking reactions and enhancing the selectivity toward 3-methoxycatechol (up to 88%). With these findings, we assessed the potential of this catalyst-free technology for a possible implementation in the field of chemistry. In this context, we identified avenues for improvement, particularly in terms of reactor productivity and energy efficiency to better align with industrial standards of the field.

Green foundation

1. We showed that the energy released during cavitation bubble collapse can be harnessed to induce the *O*-demethylation of biobased aromatics derived from lignin, without assistance of any catalyst.
2. The absence of catalysts, salts, and aqueous effluents offers major advantages over conventional catalytic processes. Furthermore, our ultrasonic reactor operates at near-room temperature and atmospheric pressure, and the reaction can also be instantly stopped, which offers additional safety benefits.
3. Transitioning from a batch system to a microfluidic reactor represents an important perspective not only to increase the reactor productivity to above 70 kg m^{-3} h^{-1}, but also to significantly reduce energy consumption, bringing it closer to industrial benchmarks (14 kJ g^{-1}).

Introduction

The urgent need to defossilize our society has opened up new avenues of research aimed at rethinking how chemical reactions are activated, ideally by harnessing renewable energy sources such as light, magnetic fields, pressure, and many others. Among the various strategies under investigation, high-frequency ultrasound is experiencing renewed interest as a means to drive chemical reactions.[1]

In essence, when a piezoelectric material is electrified, it vibrates and generates ultrasonic waves that can be transmitted into a liquid. During ultrasonic irradiation, the liquid undergoes alternating phases of compression and rarefaction.[2] If the acoustic energy is sufficiently high, it can disrupt the tensile strength of the liquid during the negative pressure cycle, resulting in the formation of gas bubbles, referred to as cavitation bubbles.[3] Due to the rectified diffusion mechanism, these bubbles absorb more gas during rarefaction than they expel during compression, causing them to grow until they can no longer withstand the surrounding pressure.[4] This leads to their violent collapse in less than a microsecond. At the collapse time, the gas inside the bubble is rapidly compressed, producing an intense localized heating effect.[5] Temperatures at the bubble–solution interface can reach several hundred degrees Celsius.[6] The density and effects of these cavitation events are strongly influenced by the applied ultrasonic frequency.[7] At low frequencies (<100 kHz), the density of cavitation bubbles is relatively low, and physical effects such as shock waves, microjets, *etc*. dominate. Conversely, at high ultrasonic frequencies, the density of cavitation bubbles is

[a]*Institut de Chimie des Milieux et Matériaux de Poitiers, Université de Poitiers, CNRS, 1 rue Marcel Doré, 86073 Poitiers, France.*
E-mail: francois.jerome@univ-poitiers.fr
[b]*Univ Montpellier, UMR 5257, ICSM, CEA, CNRS, ENSCM, Marcoule, F-30207 Bagnols Sur Cèze, France*
[c]*Eco-Efficient Products and Process Laboratory, Syensqo/CNRS, 3966 Jin Du Rd., Xin Zhuang Industrial Zone, Shanghai 201108, China*

higher but these bubbles have shorter lifetimes (less than 3 microseconds), limiting physical effects and favouring chemical effects, such as radical or cracking reactions.

Understanding the reaction mechanisms occurring at the cavitation bubble–liquid interface is crucial for evaluating the breakthrough potential of ultrasound in chemistry. However, this remains a significant scientific challenge due to the high temperature and pressure conditions reached at the bubble collapse time, which make real-time data collection using conventional spectroscopic techniques extremely difficult. We recently demonstrated that high-frequency ultrasound can induce the *N*-demethylation of *N*,*N*-dimethylaniline.[8] In particular, we showed that hydrophobic interactions can be exploited to localize cavitation bubbles in close proximity to target chemicals. Building on this finding, we selected here the *O*-demethylation of bio-based anisole-like derivatives as a model reaction to (1) gain deeper insights into the mechanisms involved at the cavitation bubble–water interface and (2) explore the possibility of controlling the selectivity of sonochemically-induced reactions. Moreover, the *O*-demethylation of bio-based anisole-like compounds is a strategically important model reaction, as aromatic compounds, particularly phenol derivatives, are industrially relevant bulk chemicals that form the basis for the synthesis of many compounds.[9] As such, this model reaction is not only relevant for mechanistic understanding, but also serves as a valuable benchmark for assessing the potential of this emerging technology in the field of chemistry.

Results and discussion

Preliminary tests

First, syringol (2,6-dimethoxyphenol) was chosen as a representative biobased methyl aryl ether. In a typical experiment, a 50 mL aqueous solution of syringol (5 mM) was subjected to ultrasonic irradiation at 550 kHz under air, while the solution temperature was maintained at 30 °C using a cooling jacket (more details in the SI, including Fig. S1). The reactivity of syringol under ultrasonic conditions was first assessed by high liquid performance chromatography (HPLC) (Fig. S2–S4).

Under these conditions, syringol was fully converted after 4 hours of ultrasonic treatment, corresponding to an initial conversion rate of approximately 1.9 mmol L^{-1} h^{-1} (Scheme 1). Syringol conversion under ultrasonic irradiation can occur *via* (1) thermal cracking at the interface of cavitation bubbles, where temperatures can reach several hundred degrees Celsius, (2) a reaction with ˙OH radicals generated by water sonolysis, or (3) a combination of both pathways. To investigate the dominant mechanism, 5,5-dimethyl-1-pyrroline-*N*-oxide (DMPO) was first added as a scavenger for ˙OH radicals (SI). Interestingly, even when added in excess (up to 0.1 M), DMPO had negligible effect on syringol conversion, suggesting that syringol is not converted into the solution by ˙OH radicals (Scheme 1). Instead, it highlights that syringol is mainly converted at the cavitation bubble–water interface, presumably mainly through a thermal cracking reaction.

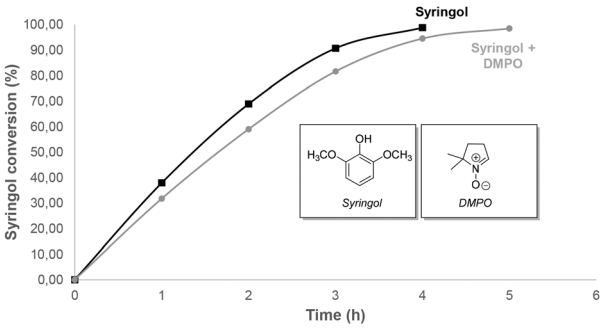

Scheme 1 Impact of DMPO on the ultrasonically-assisted conversion of syringol (550 kHz, 0.2 W mL^{-1}, 30 °C, air, 5 mM syringol, 5 mM DMPO).

To further support the occurrence of a reaction at the cavitation interface, the liquid phase was analyzed using High-Performance Liquid Chromatography (HPLC) and mass spectrometry. The nature of the primary reaction products provides additional evidence for the reaction mechanism involved. Our analytical investigations revealed that ultrasonic treatment of syringol leads to its *O*-demethylation as the primary reaction, with the detection of 3-methoxycatechol and pyrogallol (Fig. S5 and S6). The O–CH_3 bond exhibits the lowest bond dissociation energy (240 kJ mol^{-1}),[10] making it more susceptible to cleave first in hot water, thereby supporting the occurrence of cracking reactions at the cavitation bubble–water interface. At complete conversion, 3-methoxycatechol and pyrogallol were obtained in 18% and 4% yield, respectively. Other products were a mixture of various reaction products resulting from over-cracking reactions, hydroxylation, and oxidation. For instance, beside 3-methoxycatechol and pyrogallol, HPLC and ^{1}H NMR analyses of the aqueous phase (the reaction was conducted in D_2O) revealed the formation of mono-hydroxylated syringol and the oxidized adduct 2,6-dimethoxy-1,4-benzoquinone, but in lower yields, 8% and 5%, respectively (Fig. S5 and S7). These side products result from the reactions of syringol with ˙OH radicals diffusing at the cavitation bubble–water interface, further indicating that syringol itself can act as a ˙OH radical scavenger. We would like to inform readers that, in the experiments described above, the ˙OH radicals formed at the cavitation bubble–water interface are unlikely to be trapped by DMPO. Indeed, it has been shown in the literature that hydrophobic molecules tend to adsorb more strongly at the cavitation bubble–water interface.[11] Further details on this aspect are provided later in the manuscript. Based on their log *P* values (*P* being the *n*-octanol/water partition coefficient, an indicator of hydrophobicity), syringol is expected to more strongly adsorb at the cavitation bubble interface than DMPO (the log *P* values of syringol and DMPO are 1.34 and 0.02, respectively).[12] Therefore, it is more likely that DMPO captures only the fraction of ˙OH radicals diffusing into the bulk solution, whereas ˙OH radicals at the bubble interface preferentially react with syringol. Overall, these results support that syringol undergoes conversion at the cavitation bubble–

water interface predominantly *via* cracking reactions. The dominance of cracking reactions over oxidation pathways is further confirmed in the next section on optimization.

Optimization

The thermal cracking of syringol using high-frequency ultrasound is a reaction of significant interest, particularly for water depollution, as anisole-like compounds can be found in industrial aqueous effluents. However, successfully tuning the ultrasonic conditions to achieve more selective thermal cracking reactions presents an intriguing pathway to potentially convert these anisole-like pollutants into more valuable products. Although appealing, this remains a scientifically challenging task considering the extreme conditions of temperature and pressure existing at the cavitation bubble–water interface. From the previously discussed section, it appears that the decomposition of syringol is mainly thermally induced. Controlling the energy released at the cavitation bubble collapse time is thus one of the keys to prevent over-cracking reactions.

To reduce the energy released during the implosion of cavitation bubbles, the temperature of the bulk solution was varied from 16 °C to 62 °C (Scheme 2). At higher water temperatures, a greater amount of water vapors is expected to diffuse into the cavitation bubbles. Since water decomposition is an endothermic process, we hypothesize that part of the energy released during bubble collapse will be absorbed by this reaction, thereby limiting over-cracking reactions.[13] Consistent with this hypothesis, we observed that the selectivity toward *O*-demethylation products (3-methoxycatechol and pyrogallol) increased from 27% to 50% (at 40% conversion) as the temperature rose from 16 °C to 62 °C (Scheme 2).

To support that thermal cracking reactions were predominant over oxidation pathways, additional experiments were conducted. Firstly, the amount of H_2O_2, produced from the recombination of $^{\bullet}OH$ radicals, was measured both with and without syringol. In the absence of syringol, the initial formation rate of H_2O_2 was 1.50 mmol L^{-1} h^{-1}. When syringol was present, it only slightly decreased to 1.38 mmol L^{-1} h^{-1}. This indicates that approximately 0.24 mmol L^{-1} h^{-1} of $^{\bullet}OH$ radicals, ~10%, were consumed by syringol. As further evidence, the concentration of syringol was varied from 1 to 5 mM. The kinetic profiles showed no change in reaction rate or selectivity with increasing syringol concentration, supporting that $^{\bullet}OH$ radicals are not the main species involved in the conversion of syringol (Fig. S8 and Table S1). Considering that (1) the formation of cavitation bubbles appears to be the rate-determining step, and (2) the selectivity remains unchanged with varying syringol concentration, this further supports the predominance of thermal cracking reactions, otherwise the selectivity would be expected to vary.

In addition to the water temperature, the nature of the gas introduced into the solution also influenced both the conversion rate of syringol and the selectivity toward 3-methoxycatechol. The initial conversion rate of syringol followed the order: O_2 > Air > He > Ar > N_2 (Scheme 3). These variations in conversion rate can be attributed to the differences in the gases specific heat capacities, thermal conductivities, and gas solubilities in water, all of which significantly affect the density and temperature of the cavitation bubbles. Note that the higher reaction rate observed in air and O_2 can also be attributed to the increased formation of reactive oxygen species,[14] which in turn enhances the conversion of syringol through the side hydroxylation reaction and subsequent oxidation to quinone derivatives. This result is supported by the detection of monohydroxylated syringol and 2,6-dimethoxy-1,4-benzoquinone, whose combined yield is higher under air (~12%) and O_2 (~16%) compared to N_2 (~5%).

The type of gas also directly affects the selectivity of the purely thermal pathway toward 3-methoxycatechol. As discussed earlier in the context of water, diatomic gases undergo decomposition within cavitation bubbles (an endothermic process), absorbing part of the energy released during bubble collapse. As a result, higher selectivity of 3-methoxycatechol (around 40–45% at ~30% conversion) was observed under diatomic gases compared to monoatomic gases like argon and helium (around 30%), where excessive energy leads to more extensive over-cracking reactions (Scheme 4). For example, under an Ar atmosphere, partial cleavage of the Ph–OCH_3 bond in syringol was even observed, leading to the formation

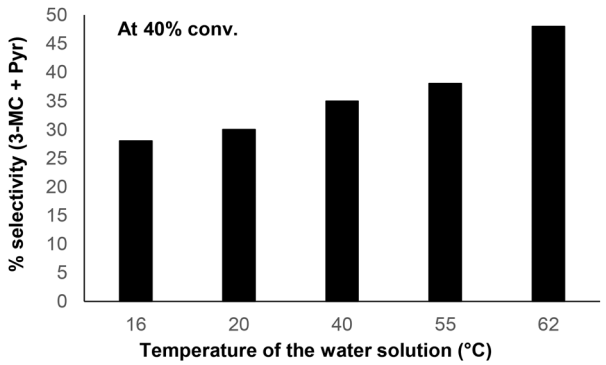

Scheme 2 Influence of the water temperature on the selectivity to (3-methhoxycatechol + pyrogallol) (550 kHz, 0.2 W mL^{-1}, air, 5 mM syringol).

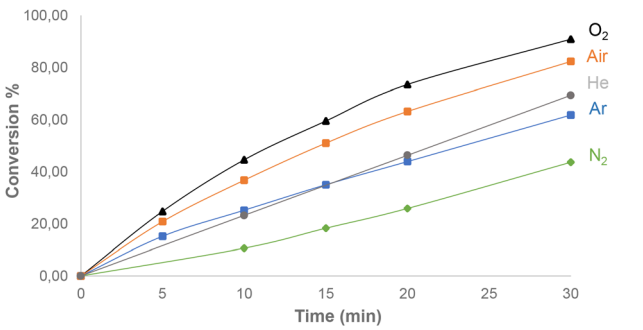

Scheme 3 Influence of the gas atmosphere on the syringol conversion (550 kHz, 0.2 W mL^{-1}, gas flow = 20 mL min^{-1}, 1 mM syringol, 50 °C).

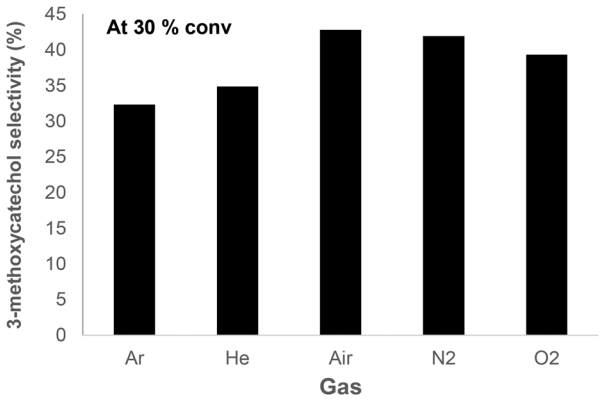

Scheme 4 Influence of the gas atmosphere on the selectivity to (3-methoxycatechol + pyrogallol) (550 kHz, 0.2 W mL^{-1}, gas flow: 20 mL min^{-1}, 1 mM syringol, 50 °C).

of trace amounts of guaiacol (<5% yield), a compound not detected under a diatomic gas atmosphere (Fig. S9). Note that, as a general trend, the selectivity of the reaction does not change significantly over the 10–90% conversion range, a result that further supports the predominant occurrence of thermal cracking of the O–CH_3 bond in syringol (Fig. S10).

With these optimized conditions in our hand, the carbon mass balance of the reaction was tentatively determined by monitoring the ultrasonic-assisted conversion of syringol over time using a Total Organic Carbon (TOC) meter. After four hours of ultrasonic irradiation at 50 °C and under air, approximately 90% of the carbon initially introduced in the form of syringol remained in the liquid phase, suggesting that 10% of the carbon escaped into the gas phase (Table S2). This finding aligns with the monodemethylation of syringol to 3-methoxycatechol and also supports the notion that other reaction products are not merely cracking products, in agreement with the detection of 2,6-dimethoxy-1,4-benzoquinone (an oxidation product of syringol) and hydroxylated syringol as described above.

To further support the above conclusion regarding thermal cracking reactions, five additional bio-based substrates derived from lignin and structurally similar to syringol were subjected to ultrasonic irradiation (550 kHz, 0.20 W mL^{-1}, air, 50 °C): 3-methoxycatechol, guaiacol, vanillin, 4-methoxyphenol and 4-methyl-2-methoxyphenol. In addition, since ethanol is increasingly employed in bio-based processes, the potential sonochemically induced cleavage of the O–C_2H_5 bond in 2-ethoxyphenol was also investigated. The results are summarized in Table 1. For all the bio-based compounds examined, including 2-ethoxyphenol, a selectivity of 30–48% toward the corresponding phenolic derivatives was observed (Table 1, entries 1–3) at about 40% conversion. This selectivity range is similar to that obtained from syringol, further supporting the

Table 1 Reactivity of various biobased "anisole-like" chemicals under high frequency ultrasound, focus on primary products[a]

Entry	Reagent	log *P* (substrate)	Conv. rate (mmol L^{-1} h^{-1})	Product	Selectivity[b] (%)
1	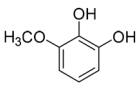	1.03	1.04	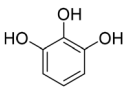	30
2	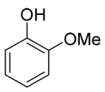	1.30	1.61		40
3	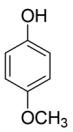	1.51	2.16	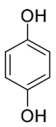	36
4		1.68	2.41		33
5	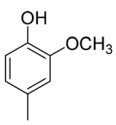	1.73	2.53	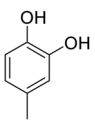	48
6	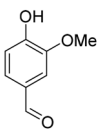	1.07	1.93	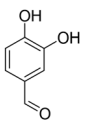	22

[a] 550 kHz, 0.20 W mL^{-1}, air, 50 °C, 1 mM substrate. [b] Selectivity was provided at 40% conversion.

hypothesis that thermal cracking of the O–alkyl bond occurs at the cavitation bubble–water interface. Indeed, in all these cases, the O–alkyl bond exhibits the lowest bond dissociation energy[10,15] and is therefore the most likely to be cleaved first under thermal conditions. Interestingly, a clear correlation was observed between the conversion rate of these bio-based substrates and their log *P* values. In other words, the higher the log *P* value, the higher the conversion rate. This finding further supports the idea that hydrophobic substrates interact more strongly at the cavitation bubble interface, where they undergo thermal cracking. Only vanillin exhibited a different behavior, showing lower selectivity (22%) and a conversion rate that does not fully correlate with its log *P* value. This deviation is attributed to side-oxidation of the aldehyde group, as confirmed by mass spectrometry (Table 1, entry 4).

Reaction mechanism

With all these data in hand, a plausible reaction mechanism can be proposed (Scheme 5). Given its log *P* value of 1.34, syringol strongly adsorbs at the surface of cavitation bubbles, primarily through hydrophobic interactions. Upon bubble collapse, the temperature at the gas–water interface rapidly rises. This induces the thermal cleavage of the O–CH_3 bond in syringol as a primary step, the bond with the lowest dissociation energy (240 kJ mol^{-1}). Due to its lower hydrophobicity (log *P* = 1.03),[16] once 3-methoxycatechol is formed near the bubble interface, it desorbs and diffuses into the bulk solution. This reduces its exposure to further thermal degradation, a notable advantage over current catalytic technologies. To support this hypothesis, an aqueous solution of 3-methoxycatechol was subjected to ultrasonication under the same conditions used for syringol (550 kHz, air, 50 °C). As expected, 3-methoxycatechol degraded at approximately half the rate of syringol, further supporting its weaker interaction with cavitation bubbles (Fig. S11).

The thermal cleavage of the O–CH_3 bond in syringol at the cavitation bubble–water interface leads to the formation of a phenoxy radical as a primary intermediate. This radical can subsequently abstract a $^{\bullet}H$ radical either from water or directly from another syringol molecule. To distinguish between these two pathways, 1,2,3-trimethoxybenzene (*i.e.* no phenolic groups) was employed as an alternative model compound. Interestingly, in this case, the overall selectivity toward 2,3- and 2.6-dimethoxyphenol (~1 : 1 ratio) dropped to 16% at 30% conversion, compared to 42% from syringol (Fig. S12 and S13). This lower selectivity suggests that the phenoxy radical formed from syringol is more likely to abstract a $^{\bullet}H$ radical from another syringol molecule rather than from water.

This mechanism also explains why the selectivity for 3-methoxycatechol levels off at around 40–50% under the optimized conditions. Inside cavitation bubbles, water vapors are partly dissociated into $^{\bullet}H$ and $^{\bullet}OH$ radicals.[17] The $^{\bullet}H$ radicals recombine to form H_2, which escapes from the reactor. At this gas–liquid interface, $^{\bullet}OH$ radicals only partially react with syringol to produce hydroxylated derivatives and the oxidized product 2,6-dimethoxy-1,4-benzoquinone or recombine to form H_2O_2.

In contrast to plasma[18] or photochemical[19] processes which predominantly depend on $^{\bullet}OH$ radical oxidation and consequently provide difficult selectivity control, unless a cock-

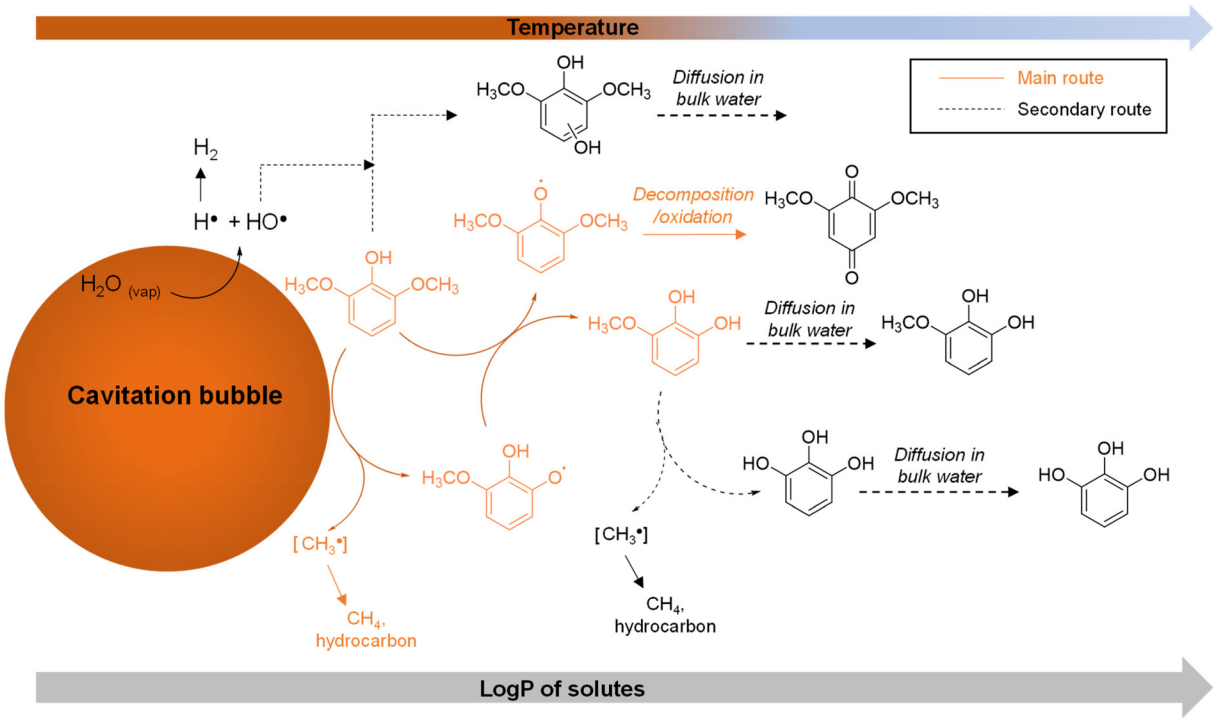

Scheme 5 Simplified illustration of the reaction mechanism.

tail mixture of reagents is used, sonochemistry offers the advantage of enhanced modulation of reaction selectivity. Indeed, the temperature reached during bubble collapse, along with the generation of $^{\bullet}OH$ (or $^{\bullet}OOH$) radicals, can be modulated by modifying the gas atmosphere or the reaction temperature, providing a means to better control the reaction selectivity.

Considering our proposed mechanism, it should theoretically be possible to enhance the selectivity towards 3-methoxycatechol by trapping the *in situ* formed phenoxy radical using a source of $^{\bullet}H$ radicals other than syringol. To evaluate this hypothesis, syringol was first subjected to ultrasonic irradiation in the presence of 2 equivalents of guaiacol. Since guaiacol and syringol have similar log *P* values, it was anticipated that both compounds would co-adsorb at the cavitation bubble–water interface, a hypothesis which was confirmed by kinetic experiments (Fig. S14). Consequently, the phenoxy radical generated from syringol would be more likely to abstract a $^{\bullet}H$ radical from guaiacol rather than from syringol itself at the interface, which should theoretically enhance the selectivity toward 3-methoxycatechol and pyrogallol. In line with this hypothesis, the presence of 2 eq. of guaiacol led to an increase in the (3-methoxycatechol + pyrogallol) selectivity from 38% to 65% (at 50% conversion), confirming that once the phenoxy radical is formed, it primarily abstracts a $^{\bullet}H$ radical from syringol (Fig. S15).

To avoid the undesired consumption of syringol or guaiacol, H_2 was bubbled into the solution with the goal of increasing the concentration of $^{\bullet}H$ radicals at the cavitation bubble–water interface, thereby promoting hydrogenation of the phenoxy radical. Additionally, H_2 is known to scavenge $^{\bullet}OH$ radicals within the cavitation bubble, which should also be beneficial for selectivity.[14] At 50 °C and at a H_2 flow rate of 20 mL min^{-1}, only a very modest improvement in selectivity toward 3-methoxycatechol was observed (44% under H_2 *vs.* 41% under N_2 at 25% conversion) (Table 2, entries 1 and 2), presumably due to the very low solubility of H_2 in water. However, when the H_2 flow rate was increased to 100 mL min^{-1}, the selectivity significantly improved to 55% and 88% at 50 °C and 60 °C, respectively (Table 2, entries 3 and 4). Notably, unlike H_2, varying the N_2 flow rate had no effect on the 3-methoxycatechol selectivity (Table 2, entry 5). This indicates that under these conditions, H_2 actively participates in the hydrogenation of the intermediate phenoxy radical, offering a promising strategy to circumvent the unwanted degradation of syringol. A summary graph showing the impact of temperature, gas flow rate, and gas atmosphere on the selectivity toward 3-methoxycatechol is presented in Fig. S16.

Table 2 Influence of the gas atmosphere on the selectivity to methoxycatechol[a]

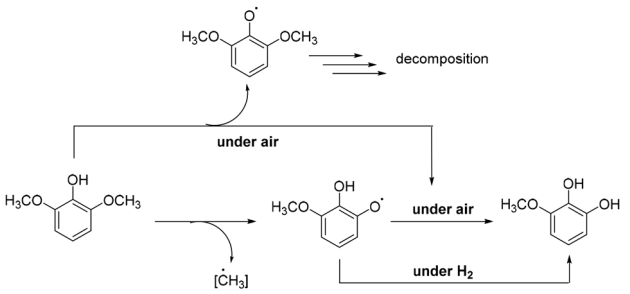

Entry	Gas	Flow rate (mL min^{-1})	Selectivity (%)
1	N_2	20	41
2	H_2	20	44
3	H_2	100	55
4	H_2	100	88[b]
5	N_2	100	39

[a] 550 kHz, 50 °C, results are given at 25% conversion. It is noteworthy that the selectivity toward 3-methoxycatechol remains relatively constant at higher levels of conversion. [b] 60 °C.

By combining all these results, we may indirectly deduce information on the state of water at the cavitation bubble periphery, and thus estimate the temperature reached at this interface. Depending on the temperature reached at the cavitation bubble interface, water can locally exhibit subcritical or supercritical conditions.[20] Under subcritical conditions, hydrolysis reactions are typically favored, leading to the release of methyl groups in the form of methanol. In contrast, supercritical conditions predominantly induce O–CH_3 bond cleavage (the weakest bond in syringol), resulting in the formation of $^{\bullet}CH_3$ radicals, which can further recombine to form gaseous hydrocarbons or CO_2 (upon *in situ* oxidation), both gases escaping the ultrasonic reactor.[21] To get more information, the fate of the CH_3 groups was traced. In this context, the experiment (under air, 50 °C, 0.2 W mL^{-1}) was repeated in D_2O and monitored using ^1H NMR (Fig. S17). Formic acid was detected in trace amounts, once again supporting that the cleavage of the –O–CH_3 bond was not induced by the $^{\bullet}OH$ radical (Table 3, entry 1). Methanol, a common hydrolysis product observed under subcritical conditions,[22] was detected in the ^1H NMR spectra. However, its quantification by ^1H NMR was not possible, as methanol likely undergoes cracking at the periphery of cavitation bubbles once formed (Table 3, entry 2).[23] Nonetheless, its presence suggests that the subcritical pathway is feasible. No other C1 compounds were detected in the liquid phase. To investigate possible cracking of syringol under supercritical conditions, the gas phase of the ultrasonic reactor was analyzed in real time using online gas chromatography (Fig. S18–S21). Methane and ethane, two markers supporting supercritical conditions, were detected, with their concentrations increasing over time (Table 3, entry 3). Additional gases such as hydrogen, originating from the sonolysis of water, as well as carbon monoxide and carbon dioxide, were also observed. The latter two suggest that $^{\bullet}CH_3$ radicals (and other degradation products) undergo oxidation with air within the cavitation bubbles.

To tentatively determine whether water was in a subcritical or supercritical state during the cleavage of the O–CH_3 bond in syringol, we correlated the observed initial syringol conversion rate with the Arrhenius plots reported by Goto for the thermal decomposition of guaiacol in both subcritical and supercritical water.[24] To align our results with Goto's work, we reproduced

Table 3 Comparison of the characteristic signatures associated with the various mechanisms at play

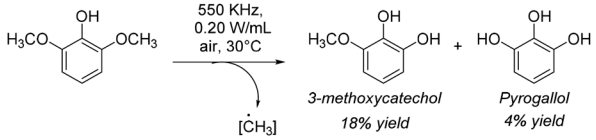

Entry	Hypothetical mechanism	Temp. estimate (°C)	Theoretical CH_3 fate	Remarks
1	$^{\bullet}OH$ radical reaction in bulk water	30	HCO_2H	Not observed
2	Subcritical water	~1200 (implausible)	MeOH	Observed
3	Supercritical water	~450	CH_4, hydrocarbon	Observed by GC

our ultrasonic experiments using guaiacol instead of syringol. Under identical ultrasonic conditions (50 °C, 0.2 W mL^{-1}, under air), the conversion rate of guaiacol was found to be very similar to that of syringol (Fig. S22). This observation is not unexpected, as the interaction between solutes and cavitation bubbles is primarily governed by hydrophobic interactions; that is, the more hydrophobic the molecule, the stronger its affinity for the gaseous cavitation bubble interfaces.[25] Okitsu reported the log *P* value as a descriptor for predicting solute–cavitation bubble interactions,[11] and since syringol and guaiacol have similar log *P* values (1.4 and 1.30 for syringol and guaiacol, respectively),[16] their comparable conversion rates are rationalized. Hence, kinetic data collected with syringol were tentatively applied to the Arrhenius equations derived by Goto for both subcritical and supercritical regimes.

Given that significantly fewer hydroxylation reactions occurred under Ar and N_2 atmospheres, kinetic profiles were examined under these two atmosphere conditions to be more accurate with the work of Goto. The calculated values of ln *k* for reactions under Ar and N_2 were −3.50 and −4.24, respectively. These values were applied to the Arrhenius equations previously reported for sub- and supercritical conditions. When using the subcritical condition equation, we obtained an implausible temperature estimate ($T > 1200$ °C), which does not align with the nature of the detected reaction products. In contrast, applying the supercritical condition equation yielded a more realistic estimated temperature of 400 ± 35 °C in Ar and 340 ± 30 °C in N_2, respectively, a temperature at which guaiacol and syringol are known to thermally decompose (Table S3 and Fig. S23).[24] Although this estimate should be interpreted with high caution, it aligns well with previous reports.[20b,26] Altogether, these results strongly support that the thermal cracking of syringol at the cavitation bubble–water interface occurs dominantly under supercritical water.

Benchmarking against current catalytic processes

The ability to control the selectivity of syringol conversion through sonochemical processes not only provides promising applications in the field of water depollution, but also raises the question of whether this technology could be extended to fine chemistry, particularly for the production of phenols from biobased feedstocks such as syringol. In the field of wastewater treatment, the potential application of high-frequency ultrasound has already been well documented and will therefore not be addressed in this section.[27] To evaluate the relevance of this technology in fine chemistry, various key performance indicators commonly used in industrial processes, such as reactor productivity, concentration, energy consumption, and selectivity, have been considered.[28]

Analysis of the current literature revealed that *O*-demethylation of aryl methyl ethers, such as anisole, can be carried out in near-critical water at temperatures around 280–300 °C, where anisole becomes miscible with water.[22] The reaction rate can be significantly enhanced in aqueous media by the addition of acid catalysts, including Brønsted acids (*e.g.*, HCl, HBr, HI, H_2SO_4) and Lewis acids (*e.g.*, $AlCl_3$, BBr_3, $B(C_6F_5)_3$).[10] In the proposed reaction mechanism, the acid, either a proton or a Lewis acid center, activates the oxygen atom, while the counter-anion (Cl^-, Br^-, I^-, *etc.*) acts as a nucleophile, attacking the methyl group. This leads to the formation of a methyl halide, which can ideally be converted into methanol under acidic aqueous conditions. These catalytic reactions, typically conducted at 250–300 °C, exhibit good selectivity (>80%) but require relatively high catalyst loadings (>50 mol%) to achieve reactor productivities in the range of 10–30 kg m^{-3} h^{-1}. When using guaiacol as the substrate, the reaction temperature can be reduced to 100–120 °C without compromising selectivity.[29] However, due to the low solubility of guaiacol in water at these lower temperatures, a very large excess of acid (>375 mol%) and a high concentration of LiBr (>61 wt% in water) are needed to facilitate the reaction. To date, in water, the most promising results have been reported by Maes in the *O*-demethylation of propyl guaiacol.[30] Under the optimized conditions, a 2 M aqueous solution of propyl guaiacol was selectively (>90%) converted to propyl catechol at 250 °C in the presence of 50 mol% HCl and under 50 bar of N_2, achieving a reactor productivity of approximately 300 kg m^{-3} h^{-1}. Based on this existing literature on the *O*-demethylation of aryl methyl ethers in water, we can identify both the main advantages and limitations of using high-frequency ultrasound.

Advantages

Among the advantages of our approach, the most significant is likely the absence of acids or salts, thus reducing the burden associated with wastewater treatment and avoiding issues

Table 4 Main advantages of our work as compared to catalytic routes

	Temp. (°C) inside the reactor	Pressure (bar) inside the reactor	Acid	Main product
Catalytic reactions	>250–300	30–50	>50 mol%	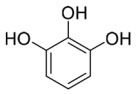
This work	30–50	1	—	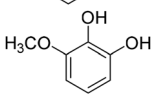

related to the corrosiveness of high-pressure reactors in the presence of large amounts of HCl (Table 4). Furthermore, despite the extreme conditions at the cavitation bubble–water interface, our ultrasonic reactor operates at near-room temperature (<50 °C) and atmospheric pressure. The reaction can also be instantly stopped by switching off the ultrasonic irradiation (on/off system, no thermal inertia involved), which offers additional safety benefits. The preferential interaction of hydrophobic molecules at the cavitation bubble interfaces also enables selective access to 3-methoxycatechol, which is nearly impossible to obtain through conventional catalytic methods (Table 4). Indeed, in syringol, both O–CH_3 bonds have comparable bond dissociation energies. Therefore, when using conventional thermal methods for syringol decomposition in hot water, it is not surprising that pyrogallol is typically the dominant product over 3-methoxycatechol.[31] Interestingly, under ultrasonic conditions, the trend was reversed. Regardless of the conversion rate, 3-methoxycatechol was consistently produced in significantly higher amounts than pyrogallol (*e.g.*, 40% *vs.* 4% at 60% conversion for high frequency ultrasound and catalysis, respectively).

Limitations and potential directions for improvement

One of the limitations is the low concentration of syringol (5 mM) compared to catalytic reactions (0.1–1.0 M) (Table 5). As above discussed, kinetic analyses revealed that the rate-determining step is the formation of cavitation bubbles (Fig. S8 and Table S1). Therefore, increasing the density of these cavitation bubbles is essential to efficiently process more concentrated syringol feeds. From a chemist perspective, this intrinsic limitation of ultrasound can be partially mitigated by taking advantage of the tendency of cavitation bubbles to interact more strongly with hydrophobic molecules than with hydrophilic ones. Specifically, if the log *P* difference between the reagent and the product is sufficiently high, it should theoretically be possible to continuously introduce the reagent into our ultrasonic reactor without degrading the reaction product. This approach would lead to a more concentrated solution of product and it would eliminate the need to remove large volumes of water at the end of the reaction, a step that is typically energy-intensive. This option is now the topic of current investigations in our group.

Table 5 Limitations and potential directions for improvement for this work

	Concentration (M)	Reactor productivity (kg m^{-3} h^{-1})
Catalytic reactions	0.1–2.00	On average 20–50 (best: 300)
This work	0.005–0.02	~1
Switch to microfluidic	0.005–0.02	Estimate > 100

The second limitation is the low productivity of the reactor (~1 kg m^{-3} h^{-1}), which is approximately 100 times lower than the industrial target (Table 5). To explore ways of increasing the ultrasonic reactor productivity, the acoustic power density was adjusted. Encouragingly, we observed that increasing the acoustic power density resulted in an exponential rise in initial syringol conversion rates (Scheme 6). Unfortunately, using our ultrasonic reactor set up, it was technically impossible to explore a higher acoustic power density than 0.2 W mL^{-1}. Assuming the hypothesis that this exponential trend can be extrapolated over a much broader range, it was estimated that an acoustic power density of 0.38 W mL^{-1} would be required to reach the industrial target of 100 kg m^{-3} h^{-1}. In other words, a high transducer area-to-water volume ratio is expected to significantly enhance the reactor productivity. Although this result should be regarded as a very rough estimate, it hypothesizes that transitioning from a batch reactor to a microfluidic ultrasonic reactor could be a promising strategy to achieve competitive reactor productivity.

Since the reactor productivity increases exponentially with acoustic power density, moving from a batch to a microfluidic reactor is also expected to significantly reduce the energy consumption of this technology. For example, by increasing the acoustic power density from 0.2 to 0.38 W mL^{-1} (corresponding to a theoretical rise in reactor productivity from 0.35 to 100 kg m^{-3} h^{-1}), the energy consumption is estimated to sharply decrease from approximately 2000 kJ g^{-1} to around 14 kJ g^{-1} of syringol (Table S4). On average, the energy con-

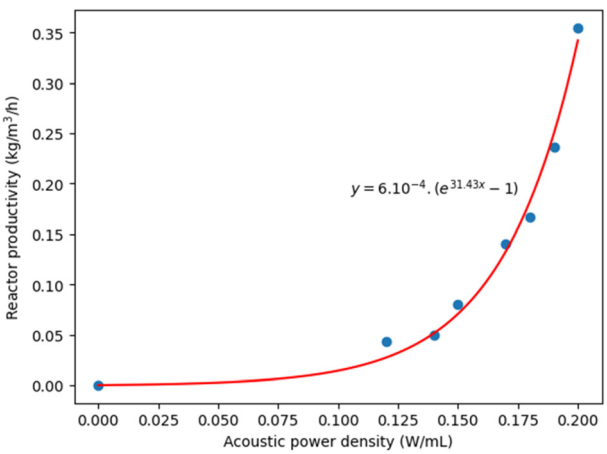

Scheme 6 Plot of the productivity as a function of acoustic power density (550 kHz, 50 °C).

sumption target at an industrial scale is lower than 20 kJ g^{-1} of product (including both reaction and downstream processing),[32] which further highlights the potential of developing microfluidic reactors for application of high frequency ultrasound in fine chemical production.

Conclusion

Using the *O*-demethylation of syringol as a model reaction, we provided in this work more information on the reaction mechanism occurring at the cavitation bubble–water interface. Kinetic data and product analyses revealed that cracking reactions mainly take place at this interface, a region where water reaches a supercritical state with an estimated temperature of around 400 ± 35 °C under our experimental conditions. Importantly, we demonstrated that the energy (temperature) released at the bubble collapse time can be partially controlled by increasing the bulk solution temperature or by introducing a diatomic gas. This approach helps to limit excessive cracking reactions, thereby enhancing the reaction selectivity to more valuable phenol derivatives. A phenoxy radical was formed as a primary product from the cleavage of the O–CH_3 bond in syringol. By bubbling hydrogen into the solution, we established a method to hydrogenate the *in situ* formed phenoxy radical, thus preventing the side consumption of syringol as a $^{\bullet}H$ radical donor and improving the reaction selectivity to as high as 88%.

Beyond mechanistic insights, these results open a potential novel pathway for the conversion of syringol into a more valuable product, 3-methoxycatechol. The absence of catalysts, salts, and aqueous effluents presents significant advantages over conventional catalytic processes. Among these, one of the most noteworthy is the reaction selectivity. While traditional catalytic routes typically lead to the simultaneous cleavage of both O–CH_3 groups in syringol, resulting in pyrogallol as the main product, our approach predominantly yields 3-methoxycatechol.

Of course, despite its breakthrough potential, the implementation of this ultrasonic technology in the field of chemistry remains a long-term goal, primarily due to its high energy consumption. Nevertheless, our work has identified promising avenues for improvement. In particular, transitioning from a batch system to a microfluidic reactor represents a key development. This shift could not only enhance the reactor productivity to an acceptable level (>70 kg m^{-3} h^{-1}), but also significantly reduce energy consumption, bringing it closer to the industrial benchmarks of the field (14 kJ g^{-1}).

Author contributions

K. Y. E. Late and D. Denis conducted the ultrasonic experiments and performed all related analyses under the supervision of P. N. Amaniampong and F. Jérôme. T. Chave provided guidance in linking the results to cavitation phenomena, while J. Delgado contributed to evaluating the industrial potential of the study.

Conflicts of interest

There are no conflicts to declare.

Data availability

The data supporting this article have been included as part of the supplementary information (SI). Supplementary information is available. See DOI: https://doi.org/10.1039/d5gc06094j.

Acknowledgements

The authors gratefully acknowledge the CNRS and the University of Poitiers for their financial support. K. Y. E. Late also acknowledges the Région Nouvelle-Aquitaine for her PhD fellowship. The authors further extend their thanks to France 2030 for funding the ECOCHEM (ANR-22-PESP-0006) and ROSALIND (ANR-24-PEBB-0010) projects, within which this study was carried out. Marie Jérôme and Léo-Paul Hauet are also acknowledged for their help in fitting the acoustic power density with the reactor productivity.

References

1 (*a*) *Sonochemistry: from Basic Principles to Innovative Applications*. Topics in Current Chemistry (2017), ed. G. Chatel and J. C. Colmenares, Springer International Publishing Switzerland, 2017; (*b*) *Characterization of Cavitation Bubbles and Sonoluminescence*, ed. R. Pflieger, S. I. Nikitenko, C. Cairos and R. Mettin, Springer, 2019; (*c*) Y. T. Didenko and K. S. Suslick, *Nature*, 2002, 394–397.
2 L. E. Kinsler, A. R. Frey, A. B. Coppens and J. V. Sanders, *in Fundamentals of acoustics*, Wiley, New York, 1982.
3 (*a*) E. A. Neppiras, *Phys. Rep.*, 1980, **61**, 159–251; (*b*) K. Yasui, in *Sonochemistry and the Acoustic Bubble*, ed. F. Grieser, P.-K. Choi, N. Enomoto, H. Harada, K. Okitsu and K. Yasui, Elsevier, Amsterdam, 2015.
4 T. Leong, M. Ashokkumar and S. Kentish, in *Handbook of Ultrasonics and Sonochemistry*, Springer, Singapore, 2016.
5 B. D. Storey and A. J. Szeri, *Proc. R. Soc. London, Ser. A*, 2001, **457**, 1685–1700.
6 (*a*) K. S. Suslick and D. J. Flannigan, *Annu. Rev. Phys. Chem.*, 2008, **59**, 659–683; (*b*) S. I. Nikitenko and R. Pflieger, *Ultrason. Sonochem.*, 2017, **35**, 623–630.
7 (*a*) A. Brotchie, F. Grieser and M. Ashokkumar, *Phys. Rev. Lett.*, 2009, **102**, 084302; (*b*) A. Dehane, S. Merouani, A. Chibani, O. Hamdaou, K. Yasui and M. Ashokkumar, *Ultrasonics*, 2022, **126**, 106824.

8 K. Late, D. Denis, Q. Blancart Remaury, P. Roszkowska, A. Grace Slater, P. N. Amaniampong, T. Chave and F. Jerome, *Green Chem.*, 2025, **27**, 7833–7842.
9 https://www.alliedmarketresearch.com/press-release/phenol-derivative-market.html.
10 X. Wu, E. Smet, F. Brandi, D. Raikwar, Z. Zhang, B. U. W. Maes and B. F. Sels, *Angew. Chem., Int. Ed.*, 2024, **63**, e202317257.
11 B. Nanzai, K. Okitsu, N. Takenaka, H. Bandow and Y. Maeda, *Ultrason. Sonochem.*, 2008, **15**, 478–483.
12 M. J. Turner III and G. M. Rosen, *J. Med. Chem.*, 1986, **29**(12), 2439–2444.
13 Y. Nakata, Y. Mizukoshi and K. Okitsu, *Ultrason. Sonochem.*, 2024, **111**, 107146.
14 M. Kohno, T. Mokudai, T. Ozawa and Y. Niwano, *J. Clin. Biochem. Nutr.*, 2011, **49**(2), 96–101.
15 W. Hu, L. Zuo, J. Liu, J. Sun and S. Wu, *BioResources*, 2016, **11**(1), 1044–1060.
16 https://www.molinspiration.com/cgi/properties.
17 (*a*) C. H. Fischer, E. J. Hart and A. Henglein, *J. Phys. Chem.*, 1986, **90**(9), 1954–1956; (*b*) S. I. Nikitenko and R. Pflieger, *Ultrason. Sonochem.*, 2017, **35**, 623–630.
18 T. Miyamoto, J. Amurao, E. Minami and H. Kawamoto, *Plasma*, 2025, **8**, 14.
19 R.-G. Hu, Y. Sang, F.-F. Tan, Y.-L. Sun, X.-S. Xue and Y. Li, *ACS Catal.*, 2023, **13**, 9264–9273.
20 (*a*) A. Henglein, *Ultrason. Sonochem.*, 1995, **2**(2), S115–S121; (*b*) H. Hung and M. R. Hoffmann, *J. Phys. Chem. A*, 1999, **103**, 2734–2739; (*c*) K. Y. Kim, K.-T. Byun and H.-Y. Kwak, *Chem. Eng. J.*, 2007, **132**(1–3), 125–135.
21 I. Graça, J. M. Lopes, M. F. Ribeiro, F. R. Ribeiro, H. S. Cerqueira and M. B. B. de Almeida, *Appl. Catal., B*, 2011, **101**(3–4), 613–621.
22 H. R. Patrick, K. Griffith, C. L. Liotta and C. A. Eckert, *Ind. Eng. Chem. Res.*, 2001, **40**, 6063–6067.
23 C. Murali Krishna, Y. Lion, T. Kondo and P. Riesz, *J. Phys. Chem.*, 1987, **91**(23), 5847–5850.
24 M. S. Wahyudiono and M. Goto, *J. Mater. Cycles Waste Manage.*, 2011, **13**, 68–79.
25 (*a*) P. Attard, *Langmuir*, 1996, **12**(6), 1693–1695; (*b*) V. Belova, D. A. Gorin, D. G. Shchukin and H. Möhwald, *ACS Appl. Mater. Interfaces*, 2011, **3**(2), 417–425; (*c*) C. J. van Oss, R. F. Giese and A. Docoslis, *J. Dispersion Sci. Technol.*, 2005, **26**, 585–590.
26 V. Mahendran, Q. Thang Trinh, X. Zhangyue, U. Jonnalagadda, T. Gould, N.-T. Nguyen, J. Kwan, T. S. Choksi, W. L. S. Valange, F. Jérôme and P. N. Amaniampong, *Angew. Chem., Int. Ed.*, 2025, **64**, e202416543.
27 (*a*) J. Fernandes, P. J. Ramísio, S. W. H. Van Hulle and H. Puga, *J. Hazard. Mater.*, 2025, **496**, 139164; (*b*) N. Lv, R. Wu, R. Guo, L. Wu, H. Zhang, C. Guo and J. Xu, *Ultrason. Sonochem.*, 2025, **112**, 107175; (*c*) P. Liu, Z. Wu, A. V. Abramova and G. Cravotto, *Ultrason. Sonochem.*, 2021, **74**, 105566.
28 J.-P. Lange, *Nat. Catal.*, 2021, **4**(3), 186–192.
29 (*a*) Z. Li, E. Sutandar, T. Goihl, X. Zhang and X. Pan, *Green Chem.*, 2020, **22**, 7989–8001; (*b*) S. B. Waghmode, G. Mahale, V. P. Patil, K. Renalson and D. Singh, *Synth. Commun.*, 2013, **1**(43), 3272–3280; (*c*) Y. Wang, M. Chen, Y. Yang, J. Ralph and X. Pan, *RSC Adv.*, 2023, **13**, 5925–5932.
30 J. Bomon, M. Bal, T. K. Achar, S. Sergeyev, X. Wu, B. Wambacq, F. Lemière, B. F. Sels and B. U. W. Maes, *Green Chem.*, 2021, **23**, 1995–2009.
31 Y. Wang, M. Chen, Y. Yang, J. Ralph and X. Pan, *RSC Adv.*, 2023, **13**, 5925–5932.
32 S. Kim and M. Overcash, *J. Chem. Technol. Biotechnol.*, 2003, **78**, 995–1005.

